Journal of Materials Chemistry C

ROYAL SOCIETY OF CHEMISTRY

PAPER

View Article Online
View Journal | View Issue

Cite this: J. Mater. Chem. C, 2022, 10, 2600

A cationic conjugated polymer with high 808 nm NIR-triggered photothermal conversion for antibacterial treatment†

Chen Zhang,‡ Kaige Wang,‡ Xueyuan Guo and Yanli Tang *

A light-triggered treatment strategy has been considered as a powerful therapeutic modality for sterilization due to its attractive properties including noninvasiveness, negligible drug resistance and minimized adverse side effects. Herein, a cationic water-soluble conjugated polymer PDTPBT based on a donor–acceptor (D–A) structure is designed and synthesized for photothermal antibacterial therapy under near-infrared light irradiation. The electron-rich dithieno-pyrrole and electron-deficient benzothiadiazole served as the electron donor and acceptor, respectively. Also, quaternary ammonium groups are modified on the side chain to enhance the water solubility of PDTPBT, promoting the effective combination of PDTPBT with bacteria. PDTPBT demonstrates a strong absorption in the near-infrared region, excellent photostability and a high photothermal conversion efficiency of up to 71.1%. High bacterial mortality rates are obtained upon 808 nm laser irradiation. Consequently, the new cationic conjugated polymer PDTPBT with excellent photothermal performance exhibited effective antibacterial ability, serving as a promising agent for light-triggered treatment.

Received 5th July 2021,
Accepted 8th September 2021

DOI: 10.1039/d1tc03128g

rsc.li/materials-c

1. Introduction

Diseases caused by pathogenic bacteria have posed a serious global challenge, which badly threatens public health security. Antibiotics play an extremely important role in antibacterial treatment over the last few decades,[1–3] which mainly depends on blocking the key process of microbial growth and reproduction.[4,5] However, due to the uncontrolled overuse of antibiotics, various drug-resistant bacteria emerged and have become another vital threat to human health. Resistance mechanisms developed by bacteria mainly include pumping out intracellular antibiotics or enzymatic degradation of antibiotics.[4,6] Besides, the dose of antibiotics needed to satisfy the sterilization effect has increased to 100 times or even 1000 times since drug-resistant genes are exchanged between bacterial populations. Although multi-antibiotic concomitant treatment achieved a better therapeutic effect in a short time, it made the problem of bacterial resistance even more serious.[4] Additionally, new antibiotics to deal with drug-resistant bacteria, such as cephalosporins and polymyxin, will eventually become ineffective.[1,7] Therefore, it is urgent to develop new antibacterial agents and methods to kill bacteria.

In recent years, light-triggered treatment strategies have been considered as an alternative therapeutic modality for sterilization, such as photothermal therapy (PTT), which is attributed to its attractive properties including noninvasiveness, negligible drug resistance, locally selective treatment and minimized adverse side effects.[1,8,9] Some photothermal agents using near infrared light (NIR) as the excitation light source have been studied, which can cause a high environmental temperature, leading to protein denaturation and cell death during heat shock.[10–14] Compared with traditional inorganic metal materials,[15–22] organic photothermal agents with good biocompatibility, low toxicity and targeted functions allow them to obtain better bactericidal performance.[1,8,11,16,23–25]

It is worth noting that conjugated polymers (CPs) have been developed as promising photothermal agents for sterilization owing to their excellent optical properties, and good light stability and light harvesting capability.[23,26–32] Among them, conjugated polymers with a D–A structure exhibit strong absorption in the NIR region due to the narrow band gap, and the low optical radiation also enables them to possess remarkable photothermal conversion efficiency.[33] However, a few water-soluble conjugated polymers in photothermal antibacterial applications have been reported.[25,27] Additionally, it is still urgent to improve the photothermal conversion efficiency of conjugated polymers for high photothermal therapy efficiency.

Key Laboratory of Applied Surface and Colloid Chemistry, Ministry of Education, Key Laboratory of Analytical Chemistry for Life Science of Shaanxi Province, School of Chemistry and Chemical Engineering, Shaanxi Normal University, Xi'an 710119, P. R. China. E-mail: yltang@snnu.edu.cn

† Electronic supplementary information (ESI) available: Synthesis of polymers, experimental procedures and supporting figures. See DOI: 10.1039/d1tc03128g

‡ These authors contributed equally to this work.

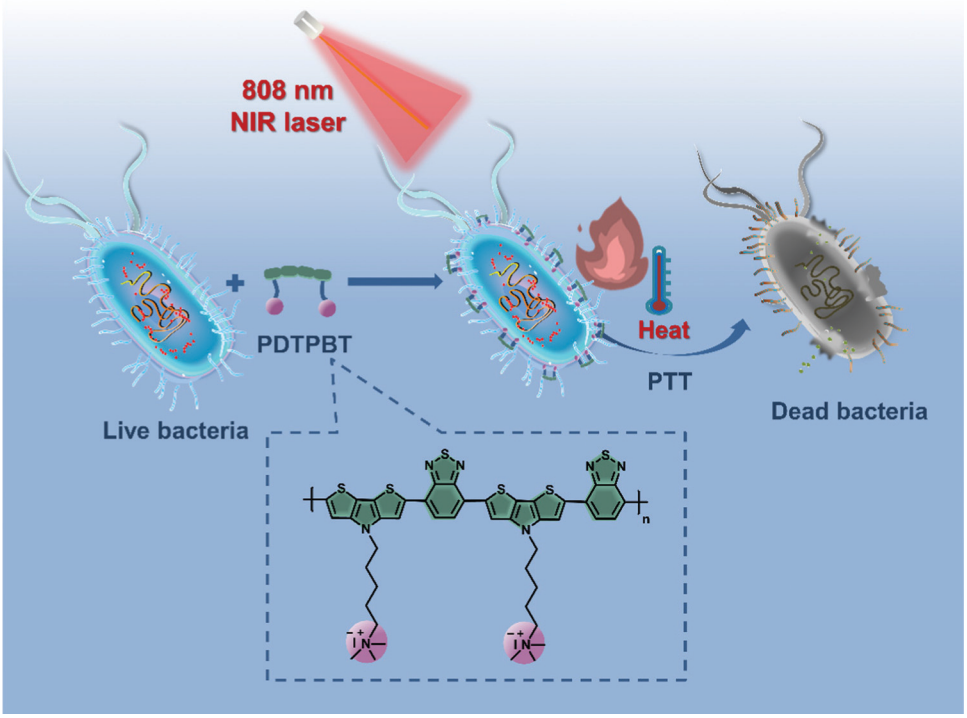

Fig. 1 The schematic photothermal antibacterial therapy mechanism of the cationic conjugated polymer PDTPBT.

Herein, a new water-soluble conjugated polymer PDTPBT with a D–A structure was designed and synthesized as a photothermal antibacterial agent, in which the electron-deficient benzothiadiazole served as the electron acceptor while the electron-rich dithieno[3,2-*b*:2′,3′-*d*]pyrrole (DTP) served as the electron donor (Fig. 1). DTP and its derivatives have also been used as important units in the construction of photovoltaic materials, which played a vital role in achieving highly efficient organic and hybrid solar cells.[34] Meanwhile, quaternary ammonium groups were modified on the side chains of conjugated polymers for better water solubility, which leads to effective contact between cationic PDTPBT and the negatively charged bacterial membrane. Importantly, PDTPBT demonstrated strong absorption in the NIR region and a remarkable photothermal conversion efficiency of up to 71.1%. Thus, the significant anti-bacterial performance towards both *E.coli* and MRSA under 808 nm laser irradiation was observed, making it a promising photothermal agent for sterilization.

2. Experimental

2.1 Materials and measurements

The reagents used in organic synthesis were purchased from Aladdin and J&K. Bacterial culture medium was obtained from Sangon Biotech. The reagents were analytically pure and used without further purification unless otherwise specified. The bacterial dyes, including Syto 9 and Syto 24, were bought from Thermo Fisher Scientific Corporation, and propidium iodide (PI) was obtained from Solarbio Life Science Corporation. The ^{1}H NMR and ^{13}C NMR spectra of the compounds were recorded using Bruker Ascend 300 or 400 MHz spectrometers. Mass spectra were recorded using a Bruker maXis II mass spectrometer (ESI†). The UV-vis spectra and fluorescence spectra were recorded on a SHIMADZU UV-2600 spectrophotometer and a Hitachi F-7000 spectrophotometer, respectively. The morphology was observed using a Hitachi SU8220 field-emission scanning electron microscope or an FEI Tecnai G2 F20 field emission transmission electron microscope. The molecular weight of the polymer was measured using a laser light scattering gel chromatography system (VISCOTEK TM, Malvern). The size distribution was measured by dynamic light scattering (DLS) (Malvern Zetasizer 3000HS). The heating processes were recorded using a thermal imager (Fluke 480 pro). The near infrared light source was bought from Changchun New Industry Optoelectronic Technology company.

2.2 Investigation of photothermal properties

808 nm laser irradiation (1 W cm^{-2}) was selected to investigate the relationship between the concentration of PDTPBT (10, 20, 50, 100, 200 μM) and the temperature of the solution within 10 min. The PDTPBT solution at 50 μM was utilized to evaluate the change in solution temperature under different irradiation conditions (0.2, 0.5, 1.0, 1.5, 2.0 W cm^{-2}). The photothermal conversion efficiency was calculated from the lifting and cooling curves. The concentration of the PDTPBT solution used was 100 μM, and the irradiation light intensity was 1 W cm^{-2}. The heating stage under laser irradiation lasted for 7 min, and the cooling stage lasted until the solution temperature dropped to room temperature. The thermal stability of PDTPBT was verified by repeating the process above 5 times consecutively.

To compare the photothermal effect between Au nanoparticles and PDTPBT, the concentration of gold nanoparticle solution was modulated to obtain the same absorbance as that of PDTPBT solution at 100 μM. The temperature changes of the two materials were recorded under the same laser intensity irradiation (1 W cm^{-2}) to obtain the lifting and cooling curves. All the heating processes can be recorded using a thermal imager.

2.3 Cytotoxicity experiments

The cytotoxicity of PDTPBT was investigated using the 3-(4,5-dimethylthiazol-2-yl)-2,5-diphenyltetrazolium bromide (MTT) assay. MCF-7 cells and 3T3 cells were selected as the representatives of tumor cells and normal cells, respectively. The suspended cells were inoculated in 96-well plates and incubated in a CO_2 incubator for 12 h. The medium was replaced with fresh full medium containing the polymer at the corresponding concentration, and the cells were cultured for 24 h. Then MTT solution (5 mg mL^{-1}) was added to each well and the cells were incubated for 4 h. After incubation, the medium was replaced by dimethyl sulfoxide (DMSO). The absorbance value of the solution in each well was read using a microplate reader at a wavelength of 490 nm.

2.4 Antibacterial experiments

The procedures of bacterial culture are shown in the ESI.† The obtained bacterial solution was centrifuged at 8000 rpm and dispersed in 0.9% NaCl solution to prepare an original bacterial solution. Then the original bacterial solution was diluted to a working concentration of 2×10^9 CFU mL^{-1} for subsequent use. The bacteria were incubated with the PDTPBT solution at different concentrations for 10 min, followed by laser irradiation for 6 min, while the control group was treated without laser irradiation. Then, mixed dyes of syto (green fluorescence) and PI (red fluorescence) were added into the solution and incubated for 15 min. The dead and live bacteria could be observed by inverted fluorescence microscopy and the bacterial mortality was measured by flow cytometry and the standard plate count method.

2.5 Study of the antibacterial mechanism

The zeta potential change of bacteria before and after photothermal treatment was examined using a nanoscale potentiometer. The bacteria were incubated with PDTPBT solution for 10 min before measurement, while the bacterial solution at a working concentration was treated without conjugated polymers as the control. A scanning electron microscope (SEM) was employed to observe the morphology of bacteria in the photothermal process to explore the bactericidal mechanism. The mixed solution was centrifuged at 8000 rpm after the sterilization step and then suspended to 2.5% glutaraldehyde solution to immobilize the cells at 4 °C overnight. The solution was centrifuged at 8000 rpm and washed with 10 mM PBS buffer. The mixed solution was dehydrated using ethanol solution (50–100%) at 4 °C for 15 min, and then dispersed in *tert*-butyl alcohol after centrifugation. Finally, a dry powder was obtained by freeze-drying and placed on the conductive adhesive for observation using a SEM.

3. Results and discussion

The synthetic route of PDTPBT is demonstrated in Fig. 2a. Compound 1 was synthesized through the Buchwald–Hartwig reaction of BINAP with 3,3′-dibromo-2,2′-bi-thiophene according to a previous report.[5,35–37] Monomer 1 was prepared by treating compound 1 with NBS (Fig. S1, ESI†). PDTPBT-pre was obtained by the Suzuki coupling reaction between monomer 1 and the bis-boronic ester of benzothiadiazole (monomer 2).[38,39] Furthermore, quaternary ammonium groups were introduced to the side chain of PDTPBT-pre by a quaternization reaction to obtain PDTPBT (Fig. S2, ESI†), enabling PDTPBT possessing better solubility. Due to the hydrophobic interactions between conjugated polymer backbones, the polymers in aqueous solution inevitably formed very loose aggregates at higher concentrations that could be affected easily by the microenvironment. The size distribution was measured by dynamic light scattering. The size was around 50–60 nm when the concentration of PDTPBT was over 10 μM (Fig. S3, ESI†). The spherical and amorphous nanoparticles can be observed from TEM images (Fig. S4, ESI†). As shown in Fig. 2b, PDTPBT showed

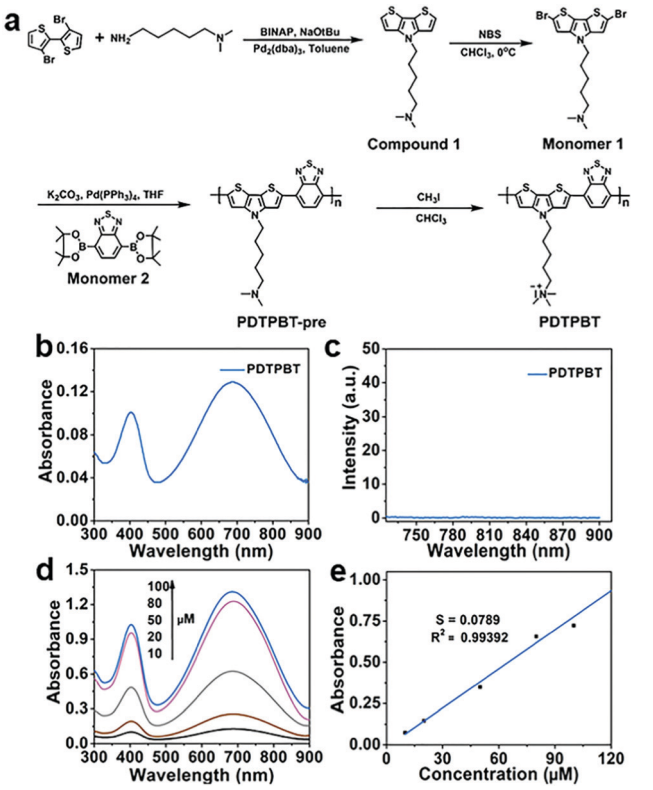

Fig. 2 (a) The synthesis of PDTPBT. (b) Absorption spectrum of PDTPBT (10^{-5} M) in aqueous solution. (c) Fluorescence spectrum of PDTPBT (10^{-6} M) in aqueous solution (λ_{ex}: 700 nm). (d) Absorption spectra of PDTPBT solution at different concentrations (10 μM to 100 μM). (e) Linear relationship between the absorbance of PDTPBT at 808 nm and PDTPBT concentrations.

an NIR absorption peak centered at 700 nm due to the D–A structure. However, as shown in Fig. 2c, no distinct emission peak can be measured, which brings the great possibility of high thermal conversion efficiency. Also, the UV-vis absorption spectra of PDTPBT at different concentrations were recorded in aqueous medium (Fig. 2d). As shown in Fig. 2e, the absorbance of the solution at 808 nm was linearly dependent on the concentration of PDTPBT in the range of 0–100 μM, enabling PDTPBT as a potential PTT agent with excellent water solubility.

The *in vitro* photothermal capability of PDTPBT was investigated at different PDTPBT concentrations. As shown in Fig. 3a and c, the temperature of the solution dramatically increased with the increase of PDTPBT concentration and irradiation time (808 nm laser) at a power density of 1 W cm^{-2}, while no remarkable temperature change was observed when pure water was exposed to the laser under the same conditions, demonstrating the potential of PDTPBT as a photothermal agent. To further examine the effect of irradiation power density on the temperature of the solution, a solution containing 50 μM PDTPBT was irradiated for 10 min with an 808 nm laser at different power intensities from 0.2 to 2 W cm^{-2}. Fig. 3b and d show that the solution temperature was dependent on the laser power and irradiation time. It reached a plateau after illumination for 6 min. The 6 min and a laser power of 1 W cm^{-2} were thus chosen as irradiation conditions for antibacterial experiments. These results demonstrated that PDTPBT can be utilized as a promising photothermal agent by controlling PDTPBT concentration or laser power to regulate the temperature of the solution, achieving effective photothermal therapy with antimicrobial and antitumor properties.

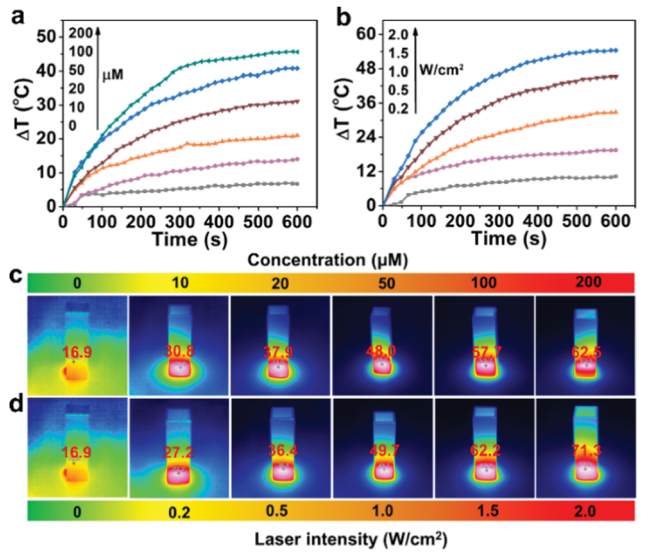

Fig. 3 (a) Temperature curves of PDTPBT at different concentrations in aqueous solutions under 808 nm laser irradiation (1 W cm^{-2}) for 10 min. (b) Temperature curves of PDTPBT (50 μM, repeated unit) in aqueous solutions under 808 nm laser irradiation at different power densities. (c) Thermographs of the PDTPBT aqueous solutions at different concentrations (ranging from 10 to 200 μM) under a NIR laser (808 nm, 1 W cm^{-2}) irradiation. (d) Thermographs of the PDTPBT aqueous (50 μM) solutions under 808 nm NIR laser irradiation at different power densities (ranging from 0.2 to 2.0 W cm^{-2}).

Furthermore, the photothermal conversion efficiency of PDTPBT was examined. As shown in Fig. 4a, the temperature increased up to 57 °C when PDTPBT solution was irradiated under 808 nm laser irradiation (1 W cm^{-2}). Then the temperature gradually decreased to room temperature. The thermal conversion efficiency was calculated using equation (1) and equation (2-4) (ESI†) reported in the literature as follows:[40–44]

$$\eta = \frac{hS\Delta T_{max} - Q_{dis}}{I(1 - 10^{-A_{808}})} \quad (1)$$

η denotes the photothermal conversion efficiency, h represents the heat transfer coefficient, S means the surface area of the container, ΔT_{max} is the temperature change between the maximum temperature reached by the sample and the ambient temperature of the surroundings. In this array, the ΔT_{max} was 32.4 °C. The container heat loss (Q_{dis}) and A_{808} were found to be 0.0454 W and 0.726, respectively. The τ means the slope of the cooling time *versus* the negative natural logarithm of the temperature. As shown in Fig. 4b, τ was obtained as 221.6 s. The other values were showed in detail in ESI†. Thus, the photothermal conversion efficiency was calculated to be 71.1%, which was higher than that of existing photothermal materials.[33,37,45,46] Presumably, the high photothermal conversion of PDTPBT may benefit from their zero radiative transition rates of the high electron-deficiency benzothiadiazole. A strong bipolaron that can decay to a phonon band may result from it, producing the thermal effect *via* nonradiative transition. Therefore, PDTPBT presents strong NIR absorption and excellent photothermal conversion efficiency, serving as a potential agent for PTT.

Photothermal stability is an important property of photothermal agents to meet the requirement of biomedical applications. The ability of PDTPBT to maintain temperature enhancement was investigated. As shown in Fig. 4c, there was no obvious change in the rising and cooling trend of the solution temperature during the five cycles of the laser (808 nm, 1 W cm^{-2}) on/off treatments. The maximum temperature of the solution increased to 57 °C during the measurement process. The results demonstrated that PDTPBT can resist long-term laser irradiation, suggesting its remarkable photothermal stability.

To compare the photothermal conversion ability, the Au nanoparticles were selected as representatives of inorganic photothermal agents. As shown in Fig. 4d, to ensure the same experimental conditions, the absorption of Au NPs and PDTPBT solution was monitored at 808 nm and was found to be the same with a value of 0.726. Then five cycles of heating and cooling processes were carried out under the same conditions. As shown in Fig. 4e and f, the solution temperature of PDTPBT increased by 33.2 °C, which was higher than that of Au NPs (22.1 °C), indicating the greater photothermal conversion capability of PDTPBT compared to Au nanoparticles.

Good biocompatibility is one of the key characteristics of photothermal agents for application in biomedical fields. As

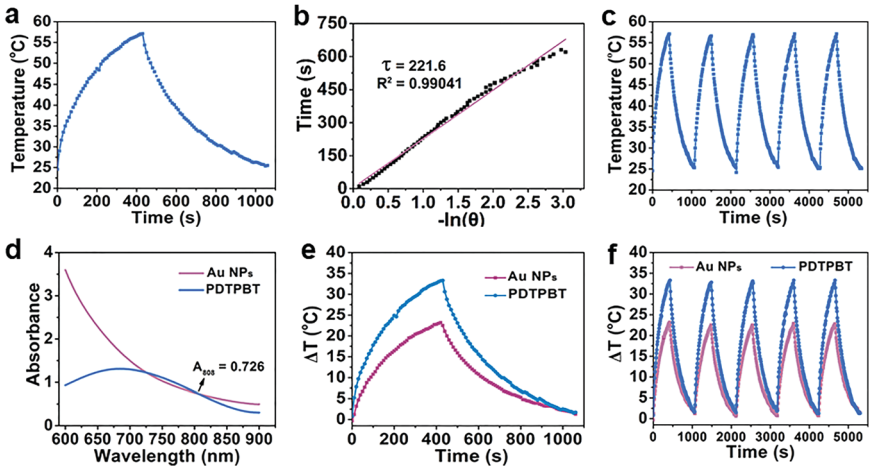

Fig. 4 (a) Photothermal effect of PDTPBT in aqueous solution (100 μM) under 808 nm laser irradiation (1 W cm^{-2}). (b) The cooling time *versus* the negative natural logarithm of the temperature obtained from the cooling stage. (c) Temperature rising and cooling profiles of the PDTPBT solution (100 μM) with irradiation on/off for five cycles. (d) UV-vis spectra of the Au NPs and PDTPBT solutions with the same absorbance at 808 nm. Temperature change (Δ*T*) profile of the Au NPs and PDTPBT solutions for (e) one cycle or (f) five cycles of the laser (808 nm, 1 W cm^{-2}) on/off treatments.

shown in Fig. 5a and b, the cell viability maintained over 84% against both MCF-7 and 3T3 cells under the experimental conditions, which indicated that PDTPBT has excellent biocompatibility. In order to explore the antibacterial activities of conjugated polymers PDTPBT against bacteria, MRSA (methicillin-resistant *Staphylococcus aureus*) and *E.coli* (*Escherichia coli*) were selected as the representatives of Gram-positive and Gram-negative bacteria, respectively. According to the reports, the enhanced temperature may cause irreversible cell damage in virtue of disrupting metabolic signals, denaturing proteins, and rupturing cell walls.[27,47] Once bacteria were incubated with PDTPBT, the cationic PDTPBT will bind with bacteria by electrostatic interactions. When the solution was exposed to laser irradiation for 6 min or kept in the dark, the viabilities of the two bacteria were determined. As shown in Fig. 5c, almost all *E.coli* bacteria were alive without laser excitation. However, the bacterial death rate significantly increased with the increase of polymer concentrations at an excitation light intensity of 1 W cm^{-2}, which resulted from lots of heat being produced by PDTPBT due to its high photothermal conversion efficiency. Fig. 5c shows that the mortality rates of *E.coli* were 75.0% and 92.8% with PDTPBT concentrations of 30 μM and 40 μM, respectively. However, the MRSA mortality rates were measured to be 8.4%, 38.2% and 92.2%, when the concentration of PDTPBT was 30 μM, 45 μM, and 60 μM, respectively (Fig. 5d). The corresponding half inhibitory concentration (IC_{50}) values of PDTPBT against *E.coli* and MRSA were 26.6 μM and 47.4 μM, respectively. Notably, the lethal concentration against *E.coli* was lower than that against MRSA due to its lower heat-resistance than MRSA.[32] These results demonstrated the remarkable sterilization effect of PDTPBT under NIR irradiation, which is promising for the treatment of pathogen infection in deep tissue.

Also, the temperature of the mixed solution of different concentrations of PDTPBT and bacteria under laser excitation was recorded by thermography. As shown in Fig. 5e, the temperature reached 63.6 °C when the concentration increased to 35 μM. In this case, *E.coli* was almost completely dead, while the mortality rate of MRSA was only 15.0% under the same

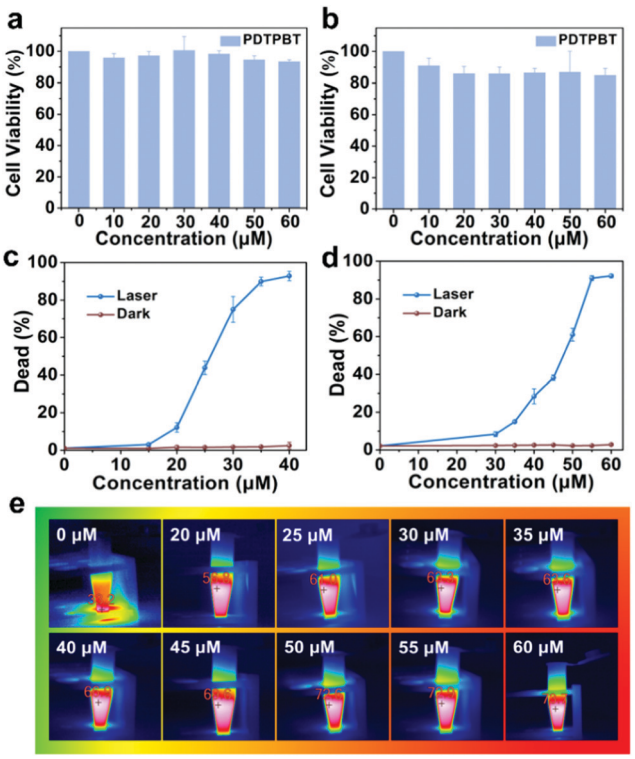

Fig. 5 Cell viability of (a) MCF-7 and (b) 3T3 incubated with PDTPBT at different concentrations in the dark for 24 h. Antibacterial activity of PDTPBT against (c) *E.coli* and (d) MRSA at different concentrations under a laser (1 W cm^{-2}) or in the dark for 6 min. The error bars represent the standard deviations of three parallel measurements. (e) Thermographs of a mixed solution of PDTPBT at different concentrations (ranging from 0 to 60 μM) and bacteria during the 6 min NIR laser (808 nm, 1 W cm^{-2}) irradiation.

conditions. When the maximum temperature of the solution increased to 73.7 °C, MRSA was completely inactive in the presence of 60 μM PDTPBT. These results further demonstrated that MRSA is more heat-resistant than *E. coli*. Additionally, the temperature of the bacteria under laser irradiation should be higher than that measured by thermography due to the direct contact between PDTPBT and bacteria, which indicated that the bacterial activity could be effectively suppressed in a brief time.[26]

In addition, the antibacterial effect of the PDTPBT polymer was investigated by the standard plate count method accordingly. After 808 nm laser illumination for 6 min, PDTPBT exhibited outstanding toxicity to *E. coli*. The number of *E.coli* colonies formed in the Petri dishes continuously decreased with an increase of the PDTPBT concentration (Fig. 6a). when the concentration of PDTPBT was 15 μM, there was no significant difference in bacterial viability between the control group and the treated group. Interestingly, the number of colonies formed in the Petri dishes decreased sharply when the concentration increased to 25 μM. Only a few colonies were observed when the PDTPBT concentration increased to 35 μM, indicating the effective inactivation of *E. coli* by PDTPBT. The corresponding experiments on MRSA were conducted (Fig. S5a, ESI†). The viability of MRSA decreased significantly when the PDTPBT concentration increased to 50 μM. These results were in accordance with the flow cytometry results (Fig. S6, ESI†).

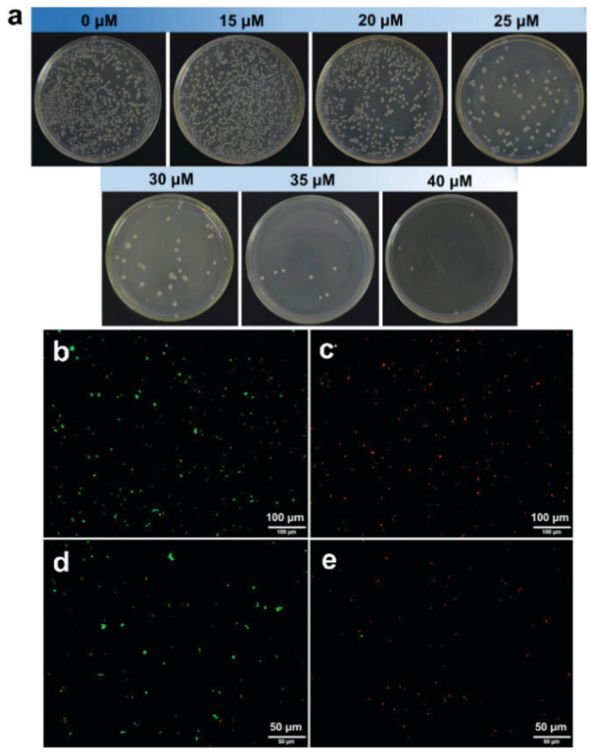

Fig. 6 (a) *E.coli* growth on Petri dishes at different concentrations of PDTPBT (ranging from 0 to 40 μM) after NIR laser (808 nm, 1 W cm^{-2}) irradiation for 6 min. Fluorescence microscopy images of *E.coli* incubated with PDTPBT under the 808 nm laser irradiation (1 W cm^{-2}) (c and e) or in the dark for 6 min (b and d). Scale bar: 100 μm (b and c), 50 μm (d and e), [PDTPBT] = 35 μM.

Table 1 The zeta potential change of *E.coli* and MRSA before and after incubation with PDTPBT

	Zeta potential (mV)	
Sample	MRSA	*E.coli*
Blank	−34.3 ± 1.3	−40.6 ± 0.5
PDTPBT	−16.0 ± 0.8	−5.3 ± 0.6

The photothermal antibacterial performance of PDTPBT against two kinds of bacteria was also investigated through confocal laser scanning microscopy. In this case, syto 9 (green) and PI (red) were used to indicate live bacteria and dead bacteria, respectively. As shown in Fig. 6b and d, the bacteria were all alive and emit green fluorescence without laser irradiation, whereas all cells emit red fluorescence when the solution was exposed to an 808 nm laser for 6 min (Fig. 6c and e), indicating dead bacteria. The same trend was found in the antibacterial investigation against MRSA (Fig. S5b–e, ESI†), indicating the remarkable PTT antibacterial effect of PDTPBT towards both Gram-positive and -negative bacteria.

To explore the mechanism of conjugated polymer sterilization, the zeta potential of bacteria before and after incubation with PDTPBT was also measured. In general, the surface of the bacteria is negatively charged due to the phospholipid coating, while PDTPBT is positively charged due to modification with quaternary ammonium groups. As shown in Table 1, before the combination with PDTPBT, the zeta potentials of *E.coli* and MRSA were −40.6 mV and −34.4 mV, respectively. After incubation with PDTPBT for 10 min, the potentials of *E.coli* and MRSA changed to −5.3 mV and −16.0 mV, respectively, which demonstrated that the zeta potential of bacteria became positive after combining with PDTPBT by dominant electrostatic interactions. It is worth noting that the zeta potential of *E.coli* changed more than MRSA, resulting from the greater binding of PDTPBT to *E.coli* cells. Thus, the stronger attachment with the polymer and poor heat resistance of *E.coli* led to a lower IC_{50} value.

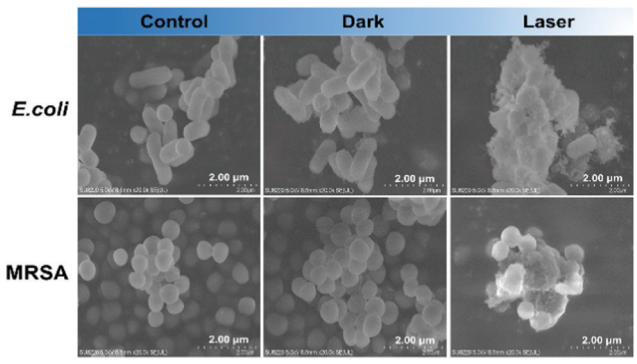

Fig. 7 SEM images of *E.coli* and MRSA incubated with PDTPBT under 808 nm laser irradiation (1 W cm^{-2}) or in the dark for 6 min. The concentrations of PDTPBT were 35 μM and 55 μM for *E.coli* and MRSA, respectively. Scale bar: 2 μm.

Additionally, scanning electron microscopy was employed to investigate the damage degree of PDTPBT to the bacteria. Fig. 7 shows that the bacterial cells both in the control groups and dark groups presented a smooth surface and complete shape. In contrast, it was clearly observed that the bacterial surface became rough and the broken cells were stuck together. Due to the large amount of heat produced by PDTPBT under laser light irradiation, the proteins in bacteria can be denatured and cell walls can be disrupted, leading to irreversible damage to the bacteria. The results illustrated that PDTPBT can efficiently kill bacteria under NIR excitation, serving as a promising PTT agent with antibacterial and antitumor properties.

4. Conclusions

In conclusion, a novel water-soluble conjugated polymer PDTPBT with a D–A structure was designed and synthesized for antibacterial therapy in this study. PDTPBT exhibited strong absorption in the near-infrared region, a remarkable photothermal conversion efficiency of up to 71.1% and excellent thermal stability. When the conjugated polymer was incubated with bacteria, PDTPBT can closely combine with bacteria by electrostatic interactions. Under 808 nm NIR laser irradiation, PDTPBT generated a large amount of heat, which caused the lysis and fusion of the cell membrane, leading to the death of bacteria. Compared with traditional photothermal materials, PDTPBT possesses excellent photothermal conversion efficiency and biocompatibility, showing a remarkable bactericidal effect. This work provides a feasible strategy for the construction of organic photothermal agents and for NIR light-controlled biomedical applications in sterilization and antitumor therapy.

Author contributions

C. Z.: data curation, methodology, and writing – original draft. K. W.: investigation, data curation, and methodology. X. G.: data curation and methodology. Y. T.: conceptualization, funding acquisition, project administration, resources, supervision, validation, and writing – review & editing.

Conflicts of interest

There are no conflicts to declare.

Acknowledgements

This work was financially supported by the National Natural Science Foundation of China (Grants 21974084 and 21675106), the Innovation Capability Support Program of Shaanxi (Program No. 2021TD-42), and the Fundamental Research Funds for the Central Universities (No. GK201901003, GK202101001).

Notes and references

1 D. Şen Karaman, U. K. Ercan, E. Bakay, N. Topaloğlu and J. M. Rosenholm, *Adv. Funct. Mater.*, 2020, **30**, 1908783.
2 B. Aslam, W. Wang, M. I. Arshad, M. Khurshid, S. Muzammil, M. H. Rasool, M. A. Nisar, R. F. Alvi, M. A. Aslam, M. U. Qamar, M. K. F. Salamat and Z. Baloch, *Infect. Drug Resist.*, 2018, **11**, 1645–1658.
3 R. Laxminarayan, P. Matsoso, S. Pant, C. Brower, J.-A. Røttingen, K. Klugman and S. Davies, *Lancet*, 2016, **387**, 168–175.
4 P. Vikesland, E. Garner, S. Gupta, S. Kang, A. Maile-Moskowitz and N. Zhu, *Acc. Chem. Res.*, 2019, **52**, 916–924.
5 Q. Cui and G. C. Bazan, *Acc. Chem. Res.*, 2018, **51**, 202–211.
6 A. Gupta, S. Mumtaz, C. H. Li, I. Hussain and V. M. Rotello, *Chem. Soc. Rev.*, 2019, **48**, 415–427.
7 S. Karanika, T. Karantanos, M. Arvanitis, C. Grigoras and E. Mylonakis, *Clin. Infect. Dis.*, 2016, **63**, 310–318.
8 P. Chen, Y. Ma, Z. Zheng, C. Wu, Y. Wang and G. Liang, *Nat. Commun.*, 2019, **10**, 1192.
9 S. Tian, H. Bai, S. Li, Y. Xiao, X. Cui, X. Li, J. Tan, Z. Huang, D. Shen, W. Liu, P. Wang, B. Z. Tang and C.-S. Lee, *Angew. Chem., Int. Ed.*, 2021, **60**, 11758–11762.
10 W. Y. Pan, C. C. Huang, T. T. Lin, H. Y. Hu, W. C. Lin, M. J. Li and H. W. Sung, *Nanomedicine*, 2016, **12**, 431–438.
11 J.-W. Xu, K. Yao and Z.-K. Xu, *Nanoscale*, 2019, **11**, 8680–8691.
12 X. Li, F. Fang, B. Sun, C. Yin, J. Tan, Y. Wan, J. Zhang, P. Sun, Q. Fan, P. Wang, S. Li and C.-S. Lee, *Nanoscale Horiz.*, 2021, **6**, 177–185.
13 Y. Chen, W. Ai, X. Guo, Y. Li, Y. Ma, L. Chen, H. Zhang, T. Wang, X. Zhang and Z. Wang, *Small*, 2019, **15**, 1902352.
14 B. Wang, G. Feng, M. Seifrid, M. Wang, B. Liu and G. C. Bazan, *Angew. Chem., Int. Ed.*, 2017, **56**, 16063–16066.
15 S. Chen, F. Tang, L. Tang and L. Li, *ACS Appl. Mater. Interfaces*, 2017, **9**, 20895–20903.
16 S. Sasidharan, R. Poojari, D. Bahadur and R. Srivastava, *ACS Sustainable Chem. Eng.*, 2018, **6**, 10562–10577.
17 C. Zhang, D. F. Hu, J. W. Xu, M. Q. Ma, H. Xing, K. Yao, J. Ji and Z. K. Xu, *ACS Nano*, 2018, **12**, 12347–12356.
18 N. G. Durmus, E. N. Taylor, K. M. Kummer and T. J. Webster, *Adv. Mater.*, 2013, **25**, 5706–5713.
19 G. Fang, W. Li, X. Shen, J. M. Perez-Aguilar, Y. Chong, X. Gao, Z. Chai, C. Chen, C. Ge and R. Zhou, *Nat. Commun.*, 2018, **9**, 129.
20 W. E. Hong, I. L. Hsu, S. Y. Huang, C. W. Lee, H. Ko, P. J. Tsai, D. B. Shieh and C. C. Huang, *J. Mater. Chem. B*, 2018, **6**, 5689–5697.
21 A. D'Agostino, A. Taglietti, R. Desando, M. Bini, M. Patrini, G. Dacarro, L. Cucca, P. Pallavicini and P. Grisoli, *Nanomaterials*, 2017, **7**, 7.
22 K. P. Steckiewicz, E. Barcinska, A. Malankowska, A. Zauszkiewicz-Pawlak, G. Nowaczyk, A. Zaleska-Medynska and I. Inkielewicz-Stepniak, *J. Mater. Sci.: Mater. Med.*, 2019, **30**, 22.
23 J. Li and K. Pu, *Chem. Soc. Rev.*, 2019, **48**, 38–71.

24 H. S. Jung, P. Verwilst, A. Sharma, J. Shin, J. L. Sessler and J. S. Kim, *Chem. Soc. Rev.*, 2018, **47**, 2280–2297.
25 Y. Ko, J. Kim, H. Y. Jeong, G. Kwon, D. Kim, M. Ku, J. Yang, Y. Yamauchi, H.-Y. Kim, C. Lee and J. You, *Carbohydr. Polym.*, 2019, **203**, 26–34.
26 Y. Han, Z. Chen, H. Zhao, Z. Zha, W. Ke, Y. Wang and Z. Ge, *J. Controlled Release*, 2018, **284**, 15–25.
27 L. Zhou, F. Lv, L. Liu and S. Wang, *Acc. Chem. Res.*, 2019, **52**, 3211–3222.
28 E. Zeglio, A. L. Rutz, T. E. Winkler, G. G. Malliaras and A. Herland, *Adv. Mater.*, 2019, **31**, 1806712.
29 H. Sun, J. Liu, S. Li, L. Zhou, J. Wang, L. Liu, F. Lv, Q. Gu, B. Hu, Y. Ma and S. Wang, *Angew. Chem., Int. Ed.*, 2019, **58**, 5988–5993.
30 Y. Yang, X. Fan, L. Li, Y. Yang, A. Nuernisha, D. Xue, C. He, J. Qian, Q. Hu, H. Chen, J. Liu and W. Huang, *ACS Nano*, 2020, **14**, 2509–2521.
31 C. Zhu, L. Liu, Q. Yang, F. Lv and S. Wang, *Chem. Rev.*, 2012, **112**, 4687–4735.
32 Y. Wang, L. Feng and S. Wang, *Adv. Funct. Mater.*, 2019, **29**, 1806818.
33 B. Bao, D. Gao, N. Li, M. Wu and C. Xing, *ACS Appl. Bio Mater.*, 2020, **3**, 2428–2437.
34 Y. Geng, A. Tang, K. Tajima, Q. Zeng and E. Zhou, *J. Mater. Chem. A*, 2019, **7**, 64–96.
35 P. Gao, D. Cho, X. Yang, V. Enkelmann, M. Baumgarten and K. Müllen, *Chem. – Eur. J.*, 2010, **16**, 5119–5128.
36 J. H. Seo, E. B. Namdas, A. Gutacker, A. J. Heeger and G. C. Bazan, *Adv. Funct. Mater.*, 2011, **21**, 3667–3672.
37 G. Feng, C.-K. Mai, R. Zhan, G. C. Bazan and B. Liu, *J. Mater. Chem. B*, 2015, **3**, 7340–7346.
38 Q. Cui and G. C. Bazan, *Acc. Chem. Res.*, 2018, **51**, 202–211.
39 Z. B. Henson, Y. Zhang, T. Nguyen, J. H. Seo and G. C. Bazan, *J. Am. Chem. Soc.*, 2013, **135**, 4163–4166.
40 Y. Cheng, Y. Chang, Y. Feng, H. Jian, Z. Tang and H. Zhang, *Angew. Chem., Int. Ed.*, 2018, **57**, 246–251.
41 C. Liu, S. Zhang, J. Li, J. Wei, K. Mullen and M. Yin, *Angew. Chem., Int. Ed.*, 2019, **58**, 1638–1642.
42 D. Wang, Y. Yao, J. He, X. Zhong, B. Li, S. Rao, H. Yu, S. He, X. Feng, T. Xu, B. Yang, T. Yong, L. Gan, J. Hu and X. Yang, *Adv. Sci.*, 2020, **7**, 1901293.
43 W. Sun, X. Zhang, H. R. Jia, Y. X. Zhu, Y. Guo, G. Gao, Y. H. Li and F. G. Wu, *Small*, 2019, **15**, 1804575.
44 L. Sun, Z. Li, R. Su, Y. Wang, Z. Li, B. Du, Y. Sun, P. Guan, F. Besenbacher and M. Yu, *Angew. Chem., Int. Ed.*, 2018, **57**, 10666–10671.
45 Y. Feng, Q. Chen, Q. Yin, G. Pan, Z. Tu and L. Liu, *ACS Appl. Bio Mater.*, 2019, **2**, 747–756.
46 H. Gao, L. Zhang, X. Lian, Y. Wang, S. Jiang, G. Wang, X. Dai, H. Zou and D. Ding, *Mater. Chem. Front.*, 2021, **5**, 3388–3395.
47 L. Liu, X. Wang, S. Zhu and L. Li, *ACS Appl. Bio Mater.*, 2021, **4**, 1211–1220.